

05

Influence of artificial notch length in composite material on damage indicator values

© A.S. Dzuba,¹ S.I. Eleonsky,¹ V.S. Pisarev,¹ A.G. Yashutin²

¹ Zhukovsky Central Aerohydrodynamic Institute, Zhukovsky, Moscow oblast, Russia

² Irkut Corporation Public Joint-Stock Company, Irkutsk, Russia

e-mail: juzzepka@mail.ru

Received December 13, 2022

Revised January 17, 2023

Accepted January 25, 2023

Novel experimental method, which provides visualization of interference fringe patterns caused by inserting of artificial notch of prefixed length in composite material, is developed. Deformation response to local material removing is measured by electronic speckle-pattern interferometry. Interferogram interpretation in terms of in-plane displacement components produces determination of two deformation parameters. These parameters represent current damage indicators, which are essential for quantitative description of damage accumulation inherent in fatigue loading of specimens with stress concentrators. Both damage indicators are derived on a base of direct physical measurements by fringe order counting. Analysis of uncertainties in damage indicators determination, which are connected with incorrect prescribing of artificial notch length, is presented.

Keywords: composite materials, speckle-pattern interferometry, artificial notch, damage indicators.

DOI: 10.21883/TP.2023.03.55808.272-22

Introduction

The study of the processes of damages accumulation, crack initiation and further development is an important step in ensuring the fatigue strength and, ultimately, the operational reliability of critical structural elements [1,2]. According to GOST 23207-78 (FATIGUE STRENGTH. TERMS, DEFINITIONS AND SYMBOLS) the fatigue damage is defined as an irreversible change in the physical and mechanical properties of an object material under the action of alternating stresses. It is natural to assume that these irreversible changes are realized through changes in the microstructure. When damages are accumulated, in most cases there is a deterioration in the performance of the structural material due to deformation processes and microstructural changes. The damage accumulation process is usually described by the damage indicator used as a variable in the kinetic equation, which characterizes the damage accumulation rate [3–6]. As such parameter a macroscopic value is used, which numerically expresses the change in damage in the studied area of the structural material.

At present, to predict the process of damage accumulation and determination, on this basis, of the moment of fatigue crack initiation, in most cases deformation, energy, phenomenological, and micromechanical models are used, which include various variables responsible for the damage occurrence at various stages of cyclic loading. Such approaches are limited in that the quantitative description of each discrete step in the process of damage accumulation requires the involvement of various parameters that cannot

be obtained by direct physical measurements [7–10]. One of the physically justified ways to identify the damage parameter can be a relative change in some specific strength characteristic. The effectiveness of this approach essentially depends on the correct choice of the damage indicator and its ability to correctly reflect the process of damage accumulation. For example, a very promising way to quantify damage accumulation is to use the evolution of the surface microstructure to predict the moment of crack initiation [11]. However, the practical application of this method encounters serious difficulties associated with errors of the characteristics measurement of the material surface microstructure at various stages of cyclic deformation.

For example, it is possible to achieve the required accuracy of indicators of damage using destructive study methods. For this, a new destructive method was developed and verified for quantitatively describe the process of damage accumulation in irregular zones of metal samples under low-cycle fatigue [12–15]. This approach is based on the use of a modified version of the method of successive crack length growth [16]. It involves samples preloading to a predetermined number of cycles and then determining the fracture mechanics parameters related to an artificial notch that is applied under a constant external load. The deformation response to local material removal in the form of a narrow notch is measured by electron speckle interferometry. In this case, notches simulating the crack serve to assess the level of fatigue damage accumulation in the same way as a probing hole used to release the energy of residual stresses in the hole drilling method [17]. The efficiency of the proposed method is illustrated in the study

of low-cycle fatigue in the vicinity of free and hardened holes in flat samples. The key point of the developed approach is that the initial experimental data, which are the tangential components of displacements in the vicinity of the notch tip, and the values of stress intensity factors (SIF) and T-stresses obtained on this basis are used as current indicators of damage. Numerical integration of dependencies describing the evolution over the life period of both non-singular (opening of notch edges and T-stress) and singular (SIF) parameters of fracture mechanics provides an explicit form of the damage accumulation function [14,15].

The approach based on the use of fracture mechanics parameters related to the artificial notch as current indicators of damage makes it possible to conduct quantitative analysis of the process of damage accumulation in metals. The use of such method for analyzing the degree of damage of composite materials, which makes it possible to assess how close the state of structural element is to the exhaustion of the deformation and strength resource, is of considerable interest. The fact is that composite materials are widely used in various industries, for example, in aircraft industry [18,19]. However, to implement the method that uses values that are measured in the vicinity of the artificial notch in the composite material, a number of technical problems must be overcome. The present paper is devoted to solving two interrelated experimental problems, namely, providing a given notch length and obtaining high-quality interference fringe patterns.

1. Objects of study

The objects of study are two flat rectangular samples with dimensions of $180 \times 30 \times t$ mm, made of composite materials with two types of packing. Both samples have a central through hole $2r_0 = 5.0$ mm in diameter, as shown

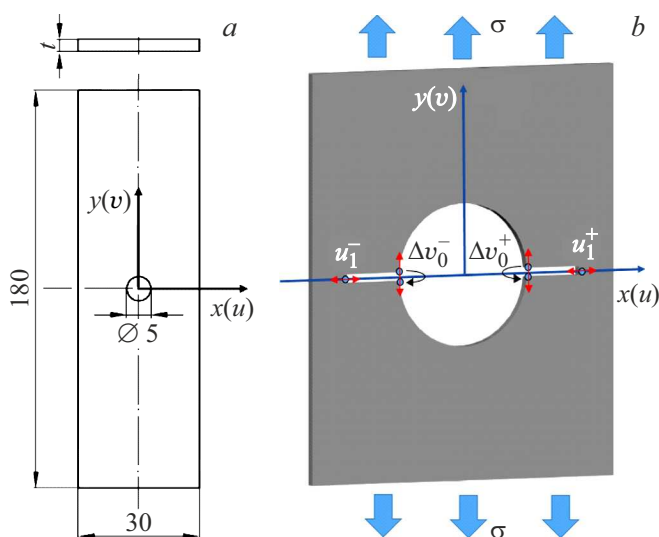


Figure 1. Scheme of the studied samples: *a* — drawing, *b* — artificial notch and damage indicators.

in Fig. 1. The initial holes were made with a carbide drill with a diameter of 4.80 mm and then reamed to diameter of $2r_0 = 5.0$ mm.

Sample S_11 is made of unidirectional carbon fiber with packing $[0_{22}]$. The thickness of the sample is $t = 4.25$ mm. The orientation of the fibers coincides with the direction of the tensile load (longitudinal modulus of elasticity). The elastic constants of the material are: longitudinal modulus of elasticity $E_1 = 138\,000$ MPa; transverse modulus of elasticity $E_2 = 7850$ MPa; shear modulus $G_{12} = 5300$ MPa; Poisson ratios $\nu_{12} = 0.25$, $\nu_{21} = 0.014$. Sample S_22 is made of longitudinal-transverse carbon composite with packing $[0/90]_{65}$. The sample thickness is $t = 4.78$ mm. The mechanical properties of the orthotropic material are: $E_1 = 73\,100$ MPa; $E_2 = 73\,100$ MPa; $G_{12} = 5300$ MPa; $\nu_{12} = \nu_{21} = 0.25$.

The generalized mechanical properties of composite materials presented above were determined on the basis of iterative numerical analysis of the vibration modes of rectangular plates caused by a point impulse impact. The main steps of this approach are as follows. At the first stage the elastic constants were determined for a thin ($t = 1.93$ mm) unidirectional composite with layers packing $[0_{10}]$. The combination of unidirectional packing and small thickness of a square plate (160×160 mm) provides a high accuracy of comparison of experimentally determined and numerically simulated vibration modes. The coincidence of the vibration modes obtained by the two methods directly determines the elastic constants of the individual layer of unidirectional composite material. These data make it possible to obtain the mechanical characteristics of the composite material with longitudinal-transverse packing, using the relations from the paper of S.G. Lekhnitskij [20]. To increase the reliability, the elastic constants of the orthotropic material were additionally determined experimentally and numerically for a rectangular plate with dimensions of $227 \times 59 \times 4.78$ mm. The mechanical characteristics of the longitudinal-transverse packing of orthotropic material obtained by the two methods show good agreement.

2. Fundamentals of the experimental approach

To make a notch under a constant tensile load, each sample is installed in the grips of the testing machine walter+bai ag, Type LFM-L 25, with a loading range of 0–25 kN. The first important point is that the loading device is included in the optical scheme of the interferometer, as shown in Fig. 2. The key feature that is needed to obtain fringe patterns is the use of a mobile module. A detailed description of this device, which is removed from the optical scheme of the interferometer for notching and then is returned to its original position with interference accuracy, is presented in [16].

Before notching each specimen is loaded with a tensile force. The value of this force must be chosen so as

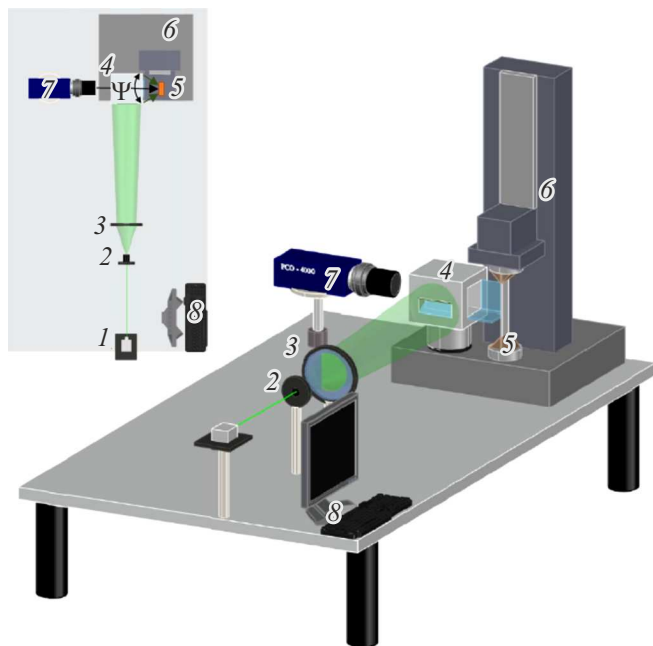


Figure 2. Interferometer circuit: 1 — diode laser, 2 — microlens, 3 — collimating lens, 4 — mobile module, 5 — sample in grips of testing machine, 6 — testing machine, 7 — video camera, 8 — PC, Ψ — angle of inclination of illuminating beams.

to provide the optimal density of the interference fringe patterns. The starting point for this choice is the experience learned in the study of metal samples with holes. Typical fringe patterns obtained by making the artificial notch from the hole contour in rectangular sample T4_09 are shown in Fig. 3.

The sample is made of 1163T aluminum alloy and has dimensions of $180 \times 30 \times 4$ mm. The diameter of the central through hole is equal to $2r_0 = 3.0$ mm. The mechanical properties of the alloy are: modulus of elasticity $E = 74\,000$ MPa; Poisson ratio $\nu = 0.33$. The fringe patterns shown in Fig. 3 were obtained for the remote stress $\sigma^M = 53.1$ MPa. The density of fringes on both images is practically optimal for determining the parameters that are used as current damage indicators [14,21]. The first indicator, shown in Fig. 1, *b*, is the value of displacement of the notch tip u_1 in the direction of the axis x . The second indicator is the opening of the notch edges at its starting point on the hole contour Δv_0 (NMOD), shown in Fig. 1, *b*. These parameters are determined as average values using the information for the right and left notches. The interference fringe patterns contain the experimental data necessary for this, as shown in Fig. 3.

The values of the parameters u_1 and Δv_0 are determined using the relations of the speckle interferometry method [22,23]:

$$u_1 = N^u \frac{\lambda}{2 \sin \Psi}, \quad \Delta v_0 = \Delta N^v \frac{\lambda}{2 \sin \Psi}, \quad (1)$$

where $\lambda = 532$ nm — wavelength of laser radiation; $\Psi = \pi/4$ — angle between inclined illumination direction and observation direction normal to the object surface; N^u is determined by direct calculation from the zero-order fringe (Fig. 3, *a*); ΔN^v is the difference in the absolute orders of the fringes, which are calculated from one fringe pattern between points located on opposite edges of the notch at its starting point (Fig. 3, *b*). Interpretation of interference fringe patterns in Fig. 3, *a*, taking into account the first formula (1), gives the following values of the first damage indicator:

$$\begin{aligned} u_1^- &= 0.38 \cdot \Delta N^{u-} = 0.38 \cdot 6.0 = 2.28 \mu\text{m}; \\ u_1^+ &= 0.38 \cdot \Delta N^{u+} = 0.38 \cdot 5.5 = 2.09 \mu\text{m}; \\ \tilde{u}_1 &= 0.38 \cdot \Delta \tilde{N}^u = 0.38 \cdot 5.75 = 2.19 \mu\text{m}. \end{aligned} \quad (2)$$

Interpretation of interference fringe patterns in Fig. 3, *b*, taking into account the second formula (1), gives the following values of the second damage indicator:

$$\begin{aligned} \Delta v_0^- &= 0.38 \cdot \Delta N_0^{v-} = 0.38 \cdot 27.0 = 10.26 \mu\text{m}; \\ \Delta v_0^+ &= 0.38 \cdot \Delta N_0^{v+} = 0.38 \cdot 27.0 = 10.26 \mu\text{m}; \\ \Delta \tilde{v}_0 &= 0.38 \cdot 27.0 = 10.26 \mu\text{m}. \end{aligned} \quad (3)$$

The density of the fringes in the fringe patterns shown in Fig. 3, as well as the values of damage indicators (2) and (3), are close to ideal parameters. The main goal of this paper is to achieve the same result for samples made of composite material. The first issue that needs to be addressed is related to the level of remote stress. To obtain an answer, it is desirable to use the minimum number of iterations, since the number of samples is always limited. The starting point is the choice of the value of the remote stress σ in relation to the moduli of elasticity of the composite and metal samples in the direction of the applied load. This ratio for unidirectional composite material is

$$E_1/E = 138\,000/74\,000 = 1.86. \quad (4)$$

The interference fringe patterns in Fig. 3 were obtained for the remote stress $\sigma^M = 53.1$ MPa. Estimate (4) gives an approximate value of the remote stress for the composite material $\sigma_0^C = 98.8$ MPa. Next, two factors must be taken into account. The first of them is the difference between the hole diameters in the metal and composite samples, namely $2r_0^M = 3.0$ mm and $2r_0^C = 5.0$ mm. It is conditionally possible to take the „first attenuation factor“ equal to $3/5 = 0.6$. The second moment of choosing external load is related to the length of the artificial incision. It is not a problem to make a notch $a_1^M \cong 2$ mm in metal material. However, for samples made of composite material, it is much more difficult to accurately make the notch $a_1^C \cong 2$ mm. The fact is that, firstly, for carrying out optical interference experiments the initial (black) surface of the samples is coated with a thin layer of mat white enamel. Secondly, the quality of the hole contour in the composite

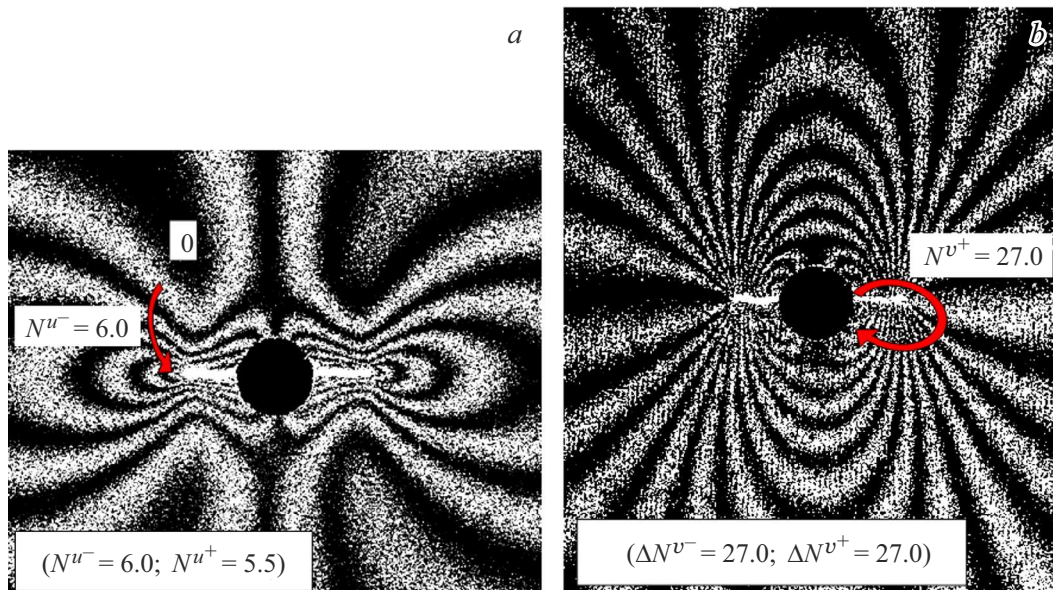


Figure 3. Sample T4_09. Interference fringe patterns obtained in terms of the flat components u (a) and v (b). Initial crack length $a_0 = 0$ with increments $\Delta a_1^- = 2.00$ mm (left notch) and $\Delta a_1^+ = 2.14$ mm (right notch). Average notch length is $\bar{a}_1 = 2.07$ mm.

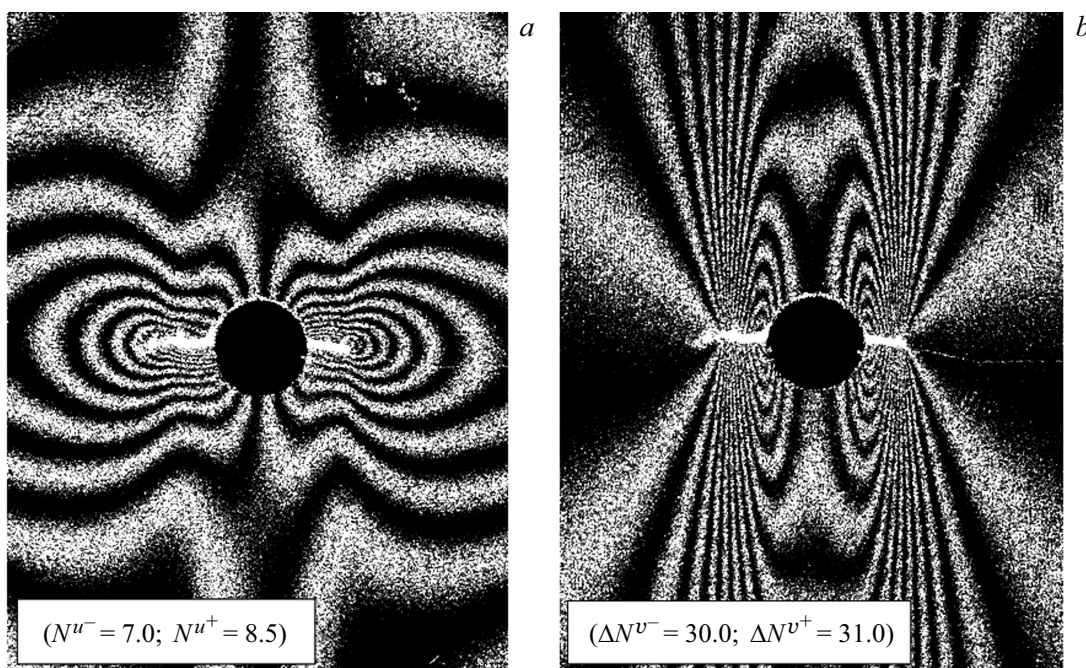


Figure 4. Sample S_11-1. Interference fringe patterns obtained in terms of the flat components u (a) and v (b). Initial notch length $a_0 = 0$ with increments $\Delta a_1^- = 2.45$ mm (left notch) and $\Delta a_1^+ = 2.17$ mm (right notch). Average notch length is $\bar{a}_1 = 2.3$ mm.

sample is worse than the quality of the hole contour in metal sample from the point of view of machining. Both of these circumstances cause difficulties in marking and lead to increase in the minimum possible length of the artificial notch. Besides, the resistance of the composite material to the action of a narrow blade of a jewelry jigsaw is much higher than that of an aluminum alloy. In the present paper an attempt is made to obtain fringe patterns

in composite sample for notch $a_1^C \cong 2.7$ mm long. The conditional „second attenuation factor“ is $2.0/2.7 = 0.74$. Thus, the „total attenuation coefficient g^C “ for choosing the remote stress level σ^C can be estimated as follows:

$$k^R = 0.6 \cdot 0.74 = 0.44. \tag{5}$$

The ratio (5) makes it possible to estimate the level of remote stress acceptable for the sample made of composite

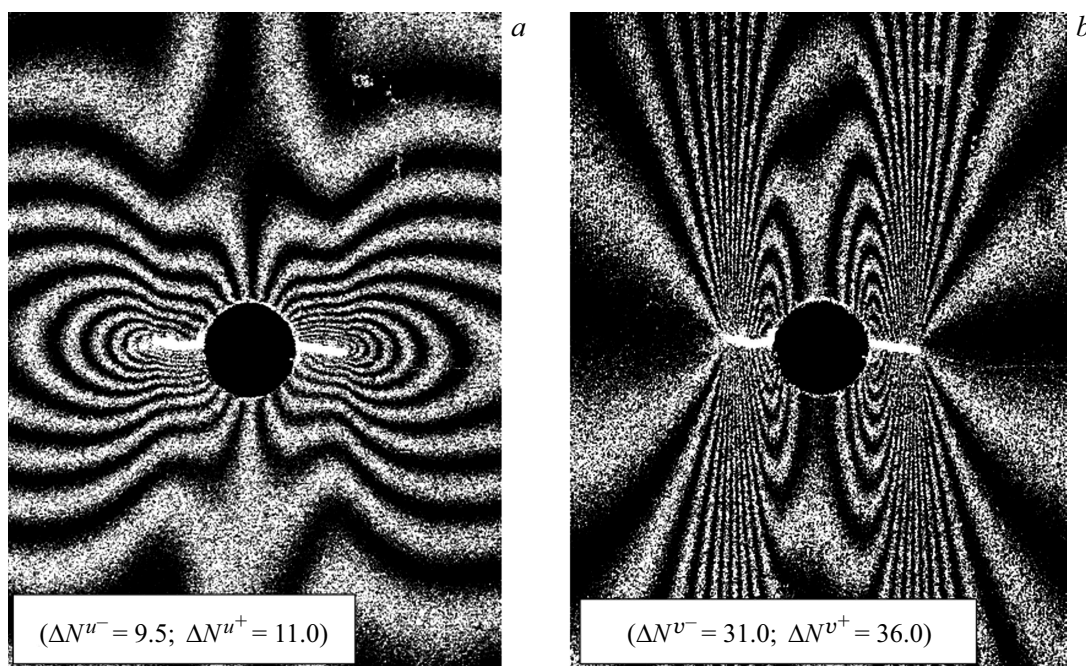


Figure 5. Sample S.11. Interference fringe patterns obtained in terms of the flat components u (a) and v (b). Initial notch length $a_0 = 0$ with increments $\Delta a_1^- = 2.66$ mm (left notch) and $\Delta a_1^+ = 2.70$ mm (right notch). Average notch length is $\tilde{a}_1 = 2.68$ mm.

material:

$$\sigma_1^C = k^R \sigma_0^C = 0.44 \cdot 98.8 = 43.5 \text{ MPa.} \quad (6)$$

Based on the estimate (6), for further experiments the value of the remote stress with a certain margin in the direction of density decreasing of the fringes was chosen equal to $\sigma^C = 39.1$ MPa.

3. Experiment method and results obtained

3.1. Unidirectional composite

The interference fringe patterns obtained as a result of making the first notch for remote stresses $\sigma^C = 39.1$ MPa are shown in Fig. 4. The beginning of the symmetrical notch $\Delta b = 0.2$ mm wide is located at two points where the sample symmetry axis (x axis) intersects with the hole contour. These fringe patterns are characterized by almost ideal quality and structure. However, note that the fringe density in Fig. 4, b reaches almost the limiting degree of resolution. Thus, the validity of the choice of the remote stress value σ^C with margin according to estimate (6) is confirmed. This means that the first sample provided the required result.

The main goal of the study is to obtain interference fringe patterns that correspond to the average notch length $\tilde{a}_1 \approx 2.70$ mm. Therefore, four sets of interference fringe patterns are recorded for one sample. The first of them corresponds to a specially underestimated value $\tilde{a}_{1-1} \approx 2.31$ mm. Then the notch length was sequentially

Table 1. Sequence of experimental procedure for Sample S.11

Numbering of incisions	a_{1-1}^-	a_{1-1}^+	–	–	–	–	–	–
a_{1-1} , mm	2.45	2.17	a_{1-1}^-	a_{1-1}^+	–	–	–	–
a_{1-2} , mm	–	–	2.45	2.70	a_{1-3}^-	a_{1-3}^+	–	–
a_{1-3} , mm	–	–	–	–	2.59	2.70	a_{1-4}^-	a_{1-4}^+
a_{1-4} , mm	–	–	–	–	–	–	2.66	2.70
\tilde{a}_1 , mm	2.31		2.58		2.65		2.68	
ΔN_0^v , bands	30.0	31.0	30.0	36.0	31.5	36.0	31.5	36.0
Δv_0 , μm	11.40	11.78	11.40	13.68	11.97	13.68	11.97	13.68
$\Delta \tilde{v}_0$, μm	11.59		12.54		12.83		12.83	
ΔN^u , bands	7.0	8.5	9.0	10.0	9.5	10.5	9.5	11.0
u_1 , μm	2.66	3.23	3.42	3.80	3.61	3.99	3.61	4.18
\tilde{u}_1 , μm	2.95		3.61		3.80		3.89	

increased only for one of the branches of the bilateral notch, reaching the total length of \tilde{a}_{1-2} , \tilde{a}_{1-3} and \tilde{a}_{1-4} . The initial state of the surface, of course, is recorded only once and is used in the visualization of all four sets of fringe patterns. The complete sequence of the implemented procedure is presented in Table 1.

The interference fringe patterns obtained as a result of applying the fourth notch are shown in Fig. 5. The right and left branches of the notch are almost equal in length. The

Table 2. Sequence of experimental procedure for Sample S_22

Numbering of incisions	a_{1-1}^-	a_{1-1}^+	-	-	-	-	-	-
a_{1-1} , mm	2.63	2.24	a_{1-2}^-	a_{1-2}^+	-	-	-	-
a_{1-2} , mm	-	-	2.63	2.77	a_{1-3}^-	a_{1-3}^+	-	-
a_{1-3} , mm	-	-	-	-	2.77	2.77	a_{1-4}^-	a_{1-4}^+
a_{1-4} , mm	-	-	-	-	-	-	2.91	2.77
\tilde{a}_1 , mm	2.43		2.70		2.77		2.84	
ΔN_0^v , bands	34.0	37.0	34.0	42.0	38.0	42.0	40.0	42.0
Δv_0 , μm	12.92	14.06	12.92	15.96	14.44	15.96	15.2	15.96
$\Delta \tilde{v}_0$, μm	13.49		14.44		15.20		15.58	
ΔN^u , bands	4.5	4.0	5.0	4.5	6.0	5.0	6.0	5.5
u_1 , μm	1.71	1.52	1.90	1.71	2.28	1.90	2.28	2.09
\tilde{u}_1 , μm	1.62		1.80		2.09		2.19	

average notch length is $\tilde{a}_1 = 2.68$ mm, which corresponds to the goal achievement. Note that the quality of the fringe pattern in Fig. 5 is not inferior to the ideal quality of the fringes in Fig. 4, although they were obtained with time delay in registration for the first and fourth notches using the same initial state. This fact clearly indicates a high degree of reliability of the developed experimental method.

3.2. Composite material with longitudinal-transverse packing

The ratio of the longitudinal moduli of elasticity of Sample S_11 and Sample S_22 is:

$$E_1^{11}/E_1^{22} = 138\,000/73\,100 = 1.89. \tag{7}$$

The use of coefficient (7) and relation (6) gives the initial estimate of the desired level of remote stress $\sigma_0^C = 23.0$ MPa. Again, as in the previous case, a certain margin is introduced in the direction of fringes density decreasing. Thus, the remote stress $\sigma^C = 21.7$ MPa is used in the experiments. The complete sequence of the implemented procedure is presented in Table 2. All notches were applied sequentially without current monitoring of the notch length. This is necessary to reduce the time of sample holding under load. Therefore, although the specified average notch length $\tilde{a}_{1-2} = 2.7$ mm was already reached at the second stage, the results for all four notch length increments are presented.

The interference fringe patterns obtained as a result of applying the fourth notch are shown in Fig. 6. The right and left branches of the notch are almost equal in length. The average notch length is $\tilde{a}_1 = 2.70$ mm, which corresponds to the goal achievement. These fringe patterns are characterized by good quality. However, note that the

fringe density in Fig. 6, *b* is somewhat redundant and reaches almost the limiting degree of resolution. Thus, the validity of the choice of the value of the remote stress σ^C with a margin aimed at reducing the fringe density according to estimates (6) and (7) is again confirmed. This means that the first sample provided the required result.

4. Results and discussion

Obtaining interference fringe patterns for the predetermined notch length is crucial in terms of quantitative analysis of damage accumulation in irregular zones of specimens made from composite materials. Previously, such method was developed and successfully applied to metals [15,16]. The essence of the proposed approach is to use a series of identical samples, each of which is loaded up to a predetermined number of cycles. This method provides a set of objects under study (flat samples with central hole) with different levels of damage accumulation. Next, for each of the samples it is necessary to determine the values of damage indicators by the method described above in this paper. The evolution of each of these parameters over the life time period is a necessary element to obtain an explicit form of the damage accumulation function. Therefore, an important issue is the assessment of errors in determining the values of damage indicators associated with the influence of the length of the artificial notch. At the same time, note that it is almost impossible to obtain notch of a given length at the first stage. The minimum required number of samples is seven.

A very lucky circumstance is that the experiments carried out refer to two limiting cases. Sample S_11 reveals the most pessimistic situation, namely the case when the desired notch length is reached only at the fourth stage. Relative errors in determining damage indicators can be estimated in the following way:

$$\begin{aligned}
 (\tilde{u}_1^{1-4} - \tilde{u}_1^{1-1})/\tilde{u}_1^{1-4} &= (3.89 - 2.95)/3.89 = 0.24; \\
 (\tilde{v}_0^{1-4} - \tilde{v}_0^{1-1})/\tilde{v}_0^{1-4} &= (12.83 - 11.59)/12.83 = 0.097.
 \end{aligned} \tag{8}$$

The errors in determining the parameters \tilde{u}_1 and $\Delta \tilde{v}_0$ are 24 and 9.7%, respectively. The presence of errors of this level, even for several of the complete set of samples under study, makes it almost impossible to provide a reliable quantitative description of the damage accumulation process.

Sample S_22 corresponds to the most optimistic situation where the desired notch length is reached in the second step. Relative errors in determining damage indicators are as follows:

$$\begin{aligned}
 (\tilde{u}_1^{1-2} - \tilde{u}_1^{1-1})/\tilde{u}_1^{1-2} &= (1.80 - 1.62)/1.80 = 0.10; \\
 (\tilde{v}_0^{1-2} - \tilde{v}_0^{1-1})/\tilde{v}_0^{1-2} &= (14.44 - 13.49)/14.44 = 0.066.
 \end{aligned} \tag{9}$$

The errors in determining the parameters \tilde{u}_1 and $\Delta \tilde{v}_0$ are 10 and 6.6%, respectively. The presence of errors of this

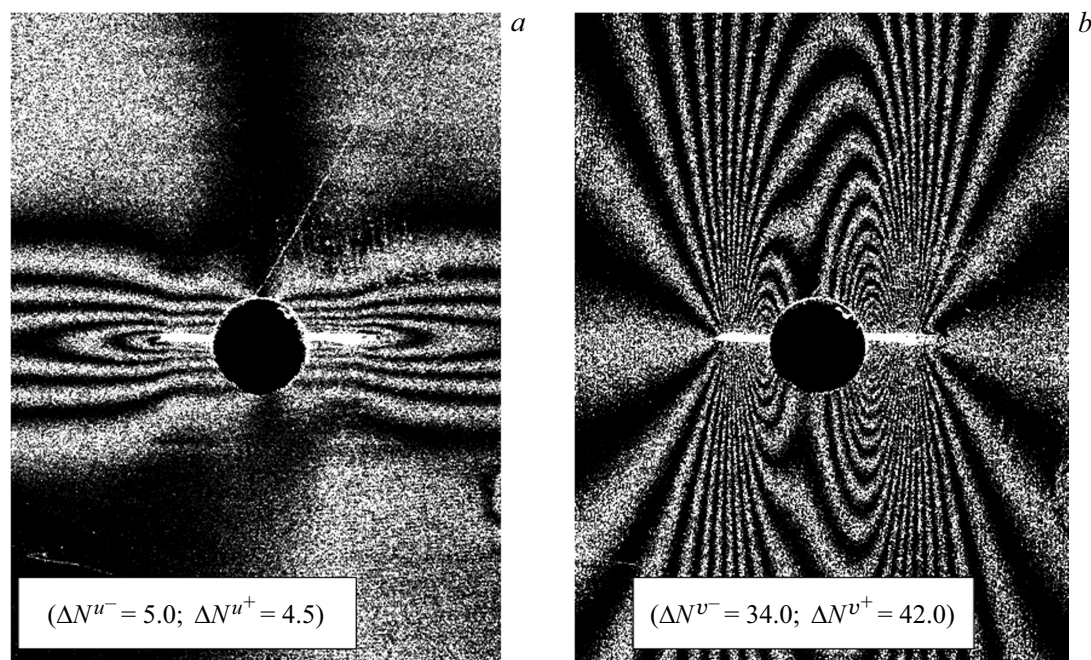


Figure 6. Sample S₂₂. Interference fringe patterns obtained in terms of the flat components u (a) and v (b). Initial notch length $a_0 = 0$ with increments $\Delta a_1^- = 2.63$ mm (left notch) and $\Delta a_1^+ = 2.77$ mm (right notch). Average notch length is $\bar{a}_1 = 2.70$ mm.

level for each of the samples under study can lead to a significant total error in determining the damage accumulation function. Thus, ensuring a constant predetermined notch length at each stage of determining the current damage indicators is an essential factor in studying the process of damage accumulation based on the destructive method.

Also important circumstance is that in order to obtain the damage accumulation function it is sufficient to use only directly measured parameters, namely, the tangential displacement components. This fact eliminates the need for a complex procedure for determining the parameters of fracture mechanics such as SIF and T-stresses, as well as taking into account the radius of the crack tip. Besides, there is no need to take into account plastic deformations at the notch tip when SIF values are determined.

An important point is that estimates (8) and (9) reveal a very high sensitivity of the used approach to change the length of the artificial notch. This means that the fringe patterns obtained make it possible to plot the distributions of two tangential displacement components directly on the edges of the artificial notch with a high degree of accuracy. This fact opens unique opportunity to verify various experimental approaches to determining the parameters of fracture mechanics for cracks propagating in structural elements made of composite materials [24–27]. These approaches use different versions of the digital image correlation method, which are characterized by lower sensitivity and spatial resolution compared to the speckle interferometry method.

Experimental information that quantitatively describes the displacement fields in the vicinity of crack in the composite material is of considerable interest from the point of view of developing and verifying numerical methods developed to determine stress intensity factors in orthotropic materials. A large number of developed approaches are based on various methods, the first stage of which includes the calculation of the displacements of points located in the immediate vicinity of the crack tip [28–31]. Besides, various force and energy criteria are widely used in the framework of numerical simulation to predict the strength of orthotropic plates of finite width with through hole [32–36]. The evolution of displacement fields, caused by a stepwise increase in the length of the notch propagating from the contour of the hole, is a necessary element to justify the choice of such criteria. Besides, the interpretation of the interference fringe patterns gives the distribution of two tangential displacement components along the edges of the notch that simulates the crack. Such information provides experimental determination of the SIF values. This, in turn, makes it possible to verify the calculation methods of SIF determining for cracks in orthotropic composite materials.

Conclusion

A new experimental method was developed that provides visualization of interference fringe patterns caused by the application of artificial notch of given length in composite material. The notch is made from the contour of the central through hole in rectangular sample when it is tensioned. Interpretation of the fringe patterns obtained

for samples with unidirectional and longitudinal-transverse packing in terms of tangential displacement components makes it possible to determine the values of two deformation parameters. These parameters are current damage indicators, which are necessary for a quantitative description of the process of damage accumulation under cyclic loading of specimens with stress concentrators. The most important fact is that both damage indicators are determined by direct physical measurements based on counting the number of interference fringes. The analysis is presented of errors in determining damage indicators, which are associated with incorrect setting of the length of the artificial notch. Two damage indicators, which are determined by making one notch, provide two damage accumulation functions. The comparison of these functions is an important factor in assessing the reliability of the final result.

Conflict of interest

The authors declare that they have no conflict of interest.

References

- [1] Yu.N. Rabotnov. *Mekhanika deformiruemogo tverdogo tela* (Nauka, Glavnaya redaktsiya Fizmatlit, M., 1979) (in Russian)
- [2] N.A. Makhutov. *Deformatsionnye kriterii razrusheniya ii raschet elementov konstruksij na prochnost* (Mashinosroenie, M., 1981) (in Russian)
- [3] V.V. Moskvitin. *Tsiklichesko nagruzhenie elementov konstruksij* (Nauka, Glavnaya redaktsiya Fizmatlit, M., 1981) (in Russian)
- [4] A.A. Movchan. *Izvestiya AN SSSR. Mekhanika tverdogo tela*, **3**, 115 (1990) (in Russian).
- [5] S. Murakami. *Continuum Damage Mechanics* (Springer Dordrecht Heidelberg London NY., 2012), DOI: 10.1007/978-94-007-2666-6
- [6] L.V. Stepanova. *Vestnik PNIPU. Mekhanika* **71**, 2008 (2020) (in Russian). DOI: 10.15593/perm.mech/2018.3.08
- [7] N.A. Makhutov. *Zavodskaya laboratoriya. Diagnostika materialov 7338* (2007). (in Russian). **66** (8), 46 (2000).
- [8] S. Elias Ferreira, J. Tupiassú Pinho de Castro, M. Antonio Meggiolaro. *Intern. J. Fatigue*, **103**, 557 (2017). <http://dx.doi.org/10.1016/j.ijfatigue.2017.06.039>
- [9] S. Elias Ferreira, J. Tupiassú Pinho de Castro, M. Intern. J. Fatigue, **115**, 89 (2018). DOI: 10.1016/j.ijfatigue.2018.03.001
- [10] N.A. Makhutov. *Zavodskaya laboratoriya. Diagnostika materialov 7338* (2007). (in Russian). **85** (9), 61 (2019).
- [11] A. Haghshenas, M.M. Khonsari. *Intern. J. Fatigue*, **107**, 130 (2017). DOI: 10.1016/j.ijfatigue.2017.10.009
- [12] Yu.G. Matvienko, V.S. Pisarev, S.I. Eleonsky. *Engineering Failure Analysis*, **106**, Article 104175 (2019). DOI: 10.1016/j.engfailanal.2019.104175
- [13] S.I. Eleonsky, Yu.G. Matvienko, V.S. Pisarev, A.V. Chernov. *Zavodskaya laboratoriya. Diagnostika materialov*, **86**, 10 (46) (in Russian).
- [14] Yu.G. Matvienko, V.S. Pisarev, S.I. Eleonsky. *Intern. J. Fatigue*, **149**, 106310 (2021). DOI: 10.1016/j.ijfatigue.2021.106310
- [15] Yu.G. Matvienko, V.S. Pisarev, S.I. Eleonsky. *Intern. J. Fatigue*, **155**, 106590 (2022). DOI: 10.1016/j.ijfatigue.2021.106590
- [16] V.S. Pisarev, Yu.G. Matvienko, S.I. Eleonsky, I.N. Odintsev. *Engineering Fracture Mechanics*, **179**, 348 (2017). DOI: 10.1016/j.engfracmech.2017.04.029
- [17] V.S. Pisarev, I.N. Odintsev, S.I. Eleonsky, A.A. Apalkov. *Opt. Laser. Engineer.*, **110**, 437 (2018). DOI: 10.1016/j.optlaseng.2018.06.022
- [18] V.I. Grishin, A.S. Dzyuba, Yu.I. Dudarkov. *Prochnost i ustojchivost elementov i soedinenij aviatsionnykh konstruksij iz kompozitov* (Izd-vo Fizmatlit, M., 2013) (in Russian)
- [19] V.I. Golovan, V.I. Grishin, A.S. Dzyuba, G.N. Zamula, M.V. Limonin, Yu.I. Dudarkov, V.S. Pisarev, K.A. Balunov. *Proektirovanie, raschety i staticheskie ispytaniya metallokompozitnykh konstruksij* (Tekhnosfera, M., 2022) (in Russian)
- [20] S.G. Lekhnitsky. *Theory of Elasticity of an Anisotropic Elastic Body* (Holden-day, Translation of 1950 Russian edition, 1963)
- [21] S.I. Eleonsky, V.S. Pisarev, D.M. Zajtsev, M.Ch. Zinchenkov, M.R. Abdullin. *Frattura ed Integritá Strutturale*, **56**, 171 (2021). DOI: 10.3221/IGF-ESIS.56.14
- [22] R. Jones, C. Wykes. *Holographic and Speckle Interferometry* (Cambridge: Cambridge Univer. Press, 1989)
- [23] P. Rastogi. *Digital Speckle Pattern Interferometry and Related Techniques* (West Sussex: John Wiley, 2001)
- [24] J.J. Dai, X. Dong Liang, X. Feng Yao, H.Y. Yeh. *J. Reinforced Plastics and Composites*, **24** (16), 1737 (2005).
- [25] S.H. Ju, S.H. Liu. *Composite Structures*, **81**, 614 (2007).
- [26] S.H. Ju, S.H. Liu, K.W. Liu. *Intern. J. Solids and Structures*, **43**, 1009 (2006).
- [27] P. Gajanan Mogadpalli, V. Parameswaran. *Strain*, **44** (6), 446 (2008). DOI: 10.1111/j.1475-1305.2007.00391.x
- [28] W.T. Chow, S.N. Atluri. *Computational Mechanics*, **21**, 1 (1998).
- [29] E. Viola, F. Tornabene, N. Fantuzzi. *Composite Structures*, **106**, 815 (2013).
- [30] L. Banks-Sills, I. Hershkovitz, P.A. Wawrzynek, R. Eliahi, A.R. Ingraffea. *Engineer. Fracture Mechanics*, **72**, 2328 (2005). DOI: 10.1016/j.engfracmech.2004.12.007
- [31] N. Fantuzzi, R. Dimitri, F. Tornabene. *Composite Structures* **145**, 162 (2016). DOI: dx.doi.org/10.1016/j.compstruct.2016.02.076
- [32] J. Hebel, W. Becker. *Mechanics of Advanced Materials and Structures*, **15** (6–7), 410 (2008).
- [33] J. Hebel, R. Dieringer, W. Becker. *Engineer. Fracture Mechanics*, **77** (18), 3558 (2010).
- [34] E. Martin, D. Leguillon, N. Carrere. *Intern. J. Solids and Structures*, **49** (26), 3915 (2012).
- [35] J. Felger, N. Stein, W. Becker. *Intern. J. Solids and Structures*, **122–123**, 14 (2017). DOI: 10.1016/j.jisols.2017.05.039
- [36] J. Felger, N. Stein, W. Becker. *Engineer. Fracture Mechanics*, **182**, 621 (2017). DOI: 10.1016/j.engfracmech.2017.05

Translated by I.Mazurov